Atmospheric Open Access
Measurement
Techniques
Discussions

A low-cost portable fibre-optic spectrometer for atmospheric absorption studies

J. Bailey

School of Physics, The University of New South Wales, NSW 2052, Australia

Correspondence to: J. Bailey (j.bailey@unsw.edu.au)

Discussion Paper | Discussion Paper | Discussion Paper | Discussion Paper |

Abstract

A compact and portable solar absorption spectrometer based on fibre-optic Fabry–Perot technology has been built and tested. The instrument weighs only 4.2 kg and operates from 5 W of power from internal batteries. It provides spectroscopy over the

range from 5980–6580 cm^{-1} (1.52–1.67 µm) at a resolution of 0.16 cm^{-1}. The input to the spectrometer is via single-mode optical fibre from a solar tracking system. Spectral scanning is carried out with a piezoelectrically scanned fibre Fabry–Perot tunable filter. Software has been developed to calibrate the spectra in wavelength and relative flux. The signal to noise ratio in solar spectra is about 700 for a spectrum scanned at

200 milliseconds per spectral point. The techniques used should be capable of being adapted to a range of wavelengths and to higher or lower resolutions.

1   Introduction

The measurement of absorption lines in the spectrum of the sun has become an important technique for studying atmospheric composition. Such measurements can determine the column density of a range of atmospheric trace gases, including important greenhouse gases such as CO_2 and CH_4. These ground-based measurements provide important data on the carbon cycle and can be used to validate space-based instruments such as SCIAMACHY (Dils et al., 2006), TANSO-FTS on GOSAT (Suto et al., 2010), and OCO-2 (Crisp, 2008).

The standard instruments used for such studies are large laboratory Fourier Transform Spectrometers (FTS) such as the Bruker IFS 125HR and similar instruments used in the Total Carbon Column Observing Network (TCCON, Wunch et al., 2011) and Network for the Detection of Atmospheric Composition Change (NDACC). These are expensive high-precision instruments requring a stable support platform, air-conditioned laboratory space and support infrastructure.

Recently there has been investigation of the possibility of making similar measurements with smaller, more portable and lower cost instruments. This could enable the establishment of larger networks and the installation of instruments in remote locations with limited infrastructure. Petri et al. (2012) and Gisi et al. (2012) have described the use of smaller, and hence lower resolution Fourier-Transform spectrometers, while Kawasaki et al. (2012) describes the use of an optical spectrum analyser (OSA) based on a grating spectrometer. However, with either a grating spectrometer or a FTS a smaller instrument generally means a lower spectral resolution.

An alternative approach is the use of a Fabry–Perot (FP) intereferometer. Because a Fabry–Perot etalon folds its light path many times through multiple reflections between two highly reflecting plates, high spectral resolutions can be achieved with a very compact optical system. A Fabry–Perot interferometer for measuring CO_2 column has been described by Wilson et al. (2007). This involved a high-order FP etalon, in which the order spacing was chosen to match the spacing of the CO_2 lines in the 1.57 µm band. A similar approach based on a fibre FP interferometer has been described by Kobayashi et al. (2010).

In contrast to these approaches which are specialist applications based on high order low finesse (5–9) etalons, the instrument described here uses a very high finesse ($\sim$ 5000) FP etalon operating in a relatively low order ($\sim$ 13). The finesse of an etalon is the ratio of its Free Spectral Range (FSR) to the full-width half maximum (FWHM) of its transmission profile. A high finesse means that a large number of independent spectral points can be scanned making the instrument a true spectrometer capable of observing substantial spectral ranges. The spectrometer described here is even more compact and portable than those mentioned above, weighing 4.2 kg, having dimensions of 35 × 25 × 11 cm, and running on internal battery power. It was built for a component cost of less than US $10 000.

2 Instrument description

A schematic diagram of the main elements of the spectrometer is given in Fig. 1. It consists of the fibre input system on the left of the diagram that is attached to a sun tracking mount and collects the light. This is connected by an optical fibre patch cord (type SMF-28 single-mode fibre from Thorlabs) to the spectrometer box itself and the spectrometer connects via a USB cable to a laptop computer used for control and data acquisition.

2.1 Fabry–Perot tunable filter

The spectrometer is based on a fibre-optic Fabry–Perot tunable filter type FFP-TF2 from Micron Optics. These devices are available with a wide range of parameters. The specifications of the tunable filter used are listed in Table 1. The device is a Fabry–Perot etalon constructed entirely in single-mode fibre, and is tuned by means of a piezoelectric transducer (PZT) that adjusts the etalon spacing and hence the transmission wavelength. The intended wavelength range of the device, as listed by the manufacturer, is 1.52–1.64 µm. However, it has been found to be usable to at least 1.67 µm with only a small loss of performance.

The tunable filter is driven by means of an applied drive voltage to the PZT in the range 0 to 60 V. Electrically the PZT is equivalent to a capacitor of about 2.2 µF, so requires a drive circuit capable of driving a high-capacitance load. The drive circuit developed for the spectrometer is based on a high-voltage operational amplifier (Texas Instruments OPA 453). To provide the wide voltage range with precisely controlled small steps, the driver is controlled by two analogue signals. A coarse signal in the range 0–6 V is amplified with a gain of 10 to generate a voltage somewhere in the 0–60 V range. The fine input has a gain of 0.5 and voltages in the range 0–10 V thus correspond to a 5 V range at the output. The two signals are summed to generate the actual drive voltage.

In operation the coarse voltage is used to set the starting point of a spectral scan, and the scan is performed by adjusting the fine voltage. Typically 1 V corresponds to about 30 cm^{-1} in spectral range.

2.2 Detector

The optical signal having passed through the FP is detected with a Femtowatt Photoreceiver model 2153 from New Focus. This uses a 1 mm diameter InGaAs PIN photodiode detector, and has a conversion gain of 2×10^{10} V W^{-1} and a noise equivalent power (NEP) of ≤ 23 fW Hz$^{-1/2}$. It is sensitive to wavelengths from 0.8 to 1.7 µm.

2.3 Computer interface

The spectrometer is interfaced to the control computer via a National Instruments (NI) USB-6211 Multifunction Data Acquisition Module. This provides two 16-bit analogue outputs that are used to generate the coarse and fine control voltages for the FP. It also has 8 differential or 16 single-ended 16-bit analogue inputs. A differential analogue input is used to measure the detector signal, and other analogue inputs are used to monitor sensor inputs and system parameters as described below. The interface module connects to the computer via a USB cable.

2.4 Power system

Power for the instrument is provided from 6 rechargeable NiMH D-cells. Voltages of +48 V and −24 V needed for the PZT driver board are generated by a small DC-DC converter. Stabilised supplies at +5 V and +15 V are generated for the USB-6211 data acquisition module and for the sensors, respectively. The USB-6211 module can be powered either from the spectrometer's internal power supply, or from the attached computer via the USB bus.

The battery voltage, current and supply voltages are monitored from the computer via analogue inputs on the USB-6211 module.

When powering both the USB-6211 module and the FP driver, the typical power consumption is 4.7 W and battery life is about 16 h. If the USB-6211 module is powered from the computer via USB, the remaining spectrometer systems use 1.8 W and battery life is about 40 h.

The detector module is powered by its own internal 9 V alkaline battery which has a lifetime of about 200 h.

2.5 Sensors

Several sensors are incorporated in the spectrometer design to provide useful ancillary information. A GPS provides latitude, longitude, altitude and UTC. A high-precision barometric pressure sensor (Setra Model 278) is also included and measures pressure to an accuracy of ±0.3 hPa with NIST traceable calibration. Temperature sensors monitor the ambient temperature, and the temperature of the FP device.

2.6 Fibre input

The fibre input unit uses an aspheric lens of 18.75 mm focal length to focus sunlight onto the fibre. The lens is sized to match the numerical aperture of the fibre. In front of the lens is an order-sorting filter. The filter is needed to isolate a single order of the FP, where the orders are spaced in wavelength by the free spectral range 0.124 µm. Three filters have been used to cover the range of the spectrometer with central wavelengths and bandwidths of 1.55 µm (0.04 µm), 1.58 µm (0.04 µm) and 1.61 µm (0.09 µm).

2.7 Sun tracker

For initial tests of the spectrometer, a low cost (< US $ 2000) sun tracker has been built using amateur astronomy hardware. It consists of a Coronado Personal Solar Telescope (PST) mounted on a Skywatcher EQ3 SynScan equatorial mount. The telescope

is fitted with a CCD camera that can monitor the solar image. The mount's SynScan controller supports a solar tracking mode, and fine adjustments to the tracking can be made based on the solar image from the camera. The fibre input unit is attached to the same mounting plate as the telescope using a kinematic mount and adjusted to be boresighted with the telescope.

While this works well as a tracker, and will track the sun to better than one minute of arc, it is considerably bulkier and heavier than the spectrometer itself. For a more portable system a compact sun tracker, such as that described by Gisi et al. (2012) would be preferable.

2.8   Control and data acquisition software

Control and data acquisition software for the spectrometer were developed using the National Instruments LabVIEW graphical programming environment. The software provides a graphical user interface for monitoring the status of the instrument and performing spectral scans. A scan is specified by the starting PZT voltage, the number of steps and the step size in volts. Two scan speeds are provided. A slow speed of one second per spectral point and a fast speed of 200 ms per point. The fast speed has normally been used for solar observations. The software provides a real time display of the spectral data during acquisition, and writes the resulting raw data to files. Each file includes in addition to the recorded spectral data, a header carrying time, position and sensor reading information for the start and end of the scan.

3   Performance and calibration

The raw data recorded by the instrument are in the form of the measured detector signal in volts at the output of the detector module, as a function of the drive voltage applied to the PZT. The data require a number of corrections to provide a calibrated spectrum.

3.1   Zero point offset

The detector does not read zero for zero illumination. It has a zero point offset which is typically in the range of −0.05 to −0.1 V. This offset is recorded by taking a dark measurement (i.e. with a cover over the optical input) of 200 points at the start and end of each spectral scan. A linear interpolation between these two measurements is then used to subtract zero point offset from each point in the spectral scan.

The zero point offset is found to vary significantly, and appears to be mostly a function of the temperature of the detector module. Figure 3 shows the offset as a function of temperature from a number of dark measurements. The temperature is not monitored at the detector module, so the temperature used in this plot is that measured at the Fabry–Perot tunable filter, which is a few centimetres away from the detector. It should be representative of the temperature at the detector, but small differences may account for some of the scatter in this diagram. Also included on this plot is a detector noise measurement from the statistics of the 200 points in each dark observation. It can be seen that both offset and noise increase with temperature, and hence cooling and stabilising the temperature of the detector module would improve its performance and stability.

After correcting for zero point the data appears as shown in Fig. 4. This represents a series of spectra recorded on 4 October 2012 with 4000 points scanned at 200 ms per spectral point (3000 points for the first scan). Such a 4000 point spectrum takes 13.33 min to record. The spectra are taken at increasing zenith angles, with the sun close to setting in the final observation.

3.2   Wavenumber calibration

While the applied drive voltage is used to control and scan the Fabry–Perot device, the relationship between voltage and wavenumber is neither linear nor stable. This is due to the property of piezoelectric actuators known as "creep". When a step voltage change is applied to the PZT a position step is performed rapidly, but the actuator

continues to move after the applied step at a rate that slowly decreases – this is the "creep". Measurable creep effects can persist for many hours after a large voltage step. In a device without closed-loop control this creep effect cannot be avoided.

The following procedure has been adopted to minimize the effects of creep in the spectrometer. Firstly the system is powered up and set to the desired starting voltage for a scan several hours before observations are attempted. The largest creep response is to the initial turn-on step from zero volts to the desired operating voltage. Then measurements on any one day are performed in a repeating pattern over the same wavenumber range. A delay of several minutes is allowed between scans to allow recovery from the step from the end position of one scan to the start position of the next.

Residual creep effects are still present, the most obvious being a slow drift of spectral features to lower voltages, that can be seen in Fig. 4, which is the creep response to the initial turn-on step. To calibrate data in wavenumber an internal calibration has to be performed for each spectral scan. This is possible because the positions of the solar and telluric lines in the spectrum are all well determined. The calibration algorithm works as follows. Firstly it locates the stronger absorption lines in the observed spectrum and measures their position in the raw spectrum as PZT voltage. This list of lines is then compared with a list of known solar and telluric lines based on line positions taken from the Kitt Peak solar atlas (Livingston and Wallace, 1991). The solar line positions are adjusted for the solar Doppler shift. A pattern-matching algorithm then selects the group of lines in the standard solar line list that best match the group containing the first 12 to 14 line positions in the observed spectrum, consistent with a set of constraints on the expected relationship between voltage and wavenumber. The process is then repeated for a new group of lines starting with the second line in the observed spectrum and so on until the last observed line is reached. This gives a number of possible identifications of each observed line, and a majority vote is used to determine the best identification.

This process will in most cases correctly identify the lines in the observed spectrum automatically. A polynomial fit is then used to fit a relationship bewteen PZT voltage and wavenumber. Typically an RMS residual to this fit of less than 0.01 cm^{-1} is obtained. Figure 5 shows the same set of data as Fig. 4 after calibration in wavenumber.

3.3 Filter response calibration

After wavenumber calibration the spectra need correction for the wavelength dependent sensitivity of the instrument. The principal contributor to this is the transmission of the interference filter used as an order sorter. The effects of this can be seen in Fig. 5 where the edges of the filter bandpass are apparent, but an additional effect is a periodic ripple in the transmission of the filter with a period of $\sim 4\,\text{cm}^{-1}$ and amplitude of $\sim 10\,\%$. Most interference filters show such an effect, even though it is not usually apparent in the manufacturer's transmission curves which are scanned at a lower resolution.

A calibration curve for this effect is derived as follows. First a model spectrum for the wavelength region scanned is made. The spectral modelling procedures used are described in Kenyi et al. (2012). The process starts with a model for the solar spectrum as seen at the top of the atmosphere which is obtained by merging the high resolution Kitt Peak solar data (Livingston and Wallace, 1991) with the lower resolution, but flux calibrated, synthetic solar spectrum of Kurucz (http://kurucz.harvard.edu/papers/irradiance/solarirr.tab). The transmission spectrum of the atmosphere is then calculated using the radiative transfer model VSTAR (Bailey and Kedziora-Chudczer, 2012) based on spectral line data from HITRAN 2008 (Rothman et al., 2009). The resulting spectrum is then convolved with the instrumental line shape model, in this case, the Airy function expected for a Fabry–Perot etalon.

The observed spectrum is then divided by the model spectrum. What is left is primarily the instrument function that is needed, but there will also be residual features due to imperfect fitting of spectral lines. Passing the divided spectrum through a low-pass Fourier filter removes all the high frequency structure due to line residuals and

leaves the low frequency structure due to the filter and ripple response. The process is illustrated in Fig. 6. By combining several of these filter response curves the response over the full range of the filter can be obtained. An example of the filter response for the 1.58 µm filter is shown in Fig. 7.

Filter response curves derived from different observations are found to agree well, and are insensitive to model parameters used in the model spectrum, provided the fitted model has a reasonable representation of the intensity of the stronger lines.

Observed spectra can then be divided by the instrument response to give final reduced spectra such as those shown in Fig. 8. Because the original solar model spectrum is flux calibrated, the resulting spectra are on a relative flux (F_ν) scale, but lack an absolute calibration because the fraction of incident sunlight received by the fibre is uncertain.

3.4 Signal to Noise Ratio

A direct estimate of the Signal to Noise Ratio (SNR) can be made by comparing observed spectra from different observations. An example of this is shown in Fig. 9 which shows a region of spectrum from 6270 to 6285 cm^{-1} from three observed spectra from the full sequence shown in Fig. 8. The upper panel shows the three spectra overlaid in black, green and red. The lower panel shows the differences (green–black) and (red–black). Some spectral lines show as weak features in the difference spectra as these are telluric lines whose strength increases due to the changing zenith angle. The solar lines do not show any change between the three spectra. The lower panel shows the noise level in the spectra and shows that this is relatively constant through the solar spectral features. From the statistics of the difference plots in regions between telluric features, a standard deviation of 0.00243 and 0.00238 is obtained for the two cases plotted. Since this is the difference bewteen two observations the noise level on a single spectrum will be a factor of $\sqrt{2}$ lower giving 0.00171 or 0.00168. Relative to the continuum level of 1.24 in the same (arbitrary) flux units, this gives a SNR ~ 730.

Almost the same value is obtained if the noise is measured from the dark measurements on either side of a scan, and the signal is measured from the spectral scan between them. For example for the 05:13 UTC observation from Fig. 5 the measured noise is 1.66 mV, and the continuum signal is around 1.17 V giving a SNR ~ 700. This indicates that the SNR is determined almost entirely by the noise of the detector module. The temperature dependence shown in Fig. 3 then indicates that better SNR will be achieved in lower temperature conditions. The figures quoted above were obtained at a temperature of $\sim 32\,°C$. The noise values in Fig. 3 are lower than those quoted above as they were measured with 1 s integrations, rather than the 200 ms integrations used in the actual observations.

Based on the manufacturer's stated conversion gain for the detector module of $2 \times 10^{10}\,V\,W^{-1}$ and the typical observed solar signal with the spectrometer of about 1 V, the detected power is $\sim 50\,pW$. The SNR due to photon shot noise at this power level is ~ 9000. This is much higher than the observed SNR of ~ 700 and confirms that the instrument is detector noise limited.

The SNR of ~ 700 is comparable with that of ~ 900 reported by Washenfelder et al. (2006) for the TCCON system. Analysis of the TCCON error budget by Wunch et al. (2011) shows that the random noise on the spectra is a relatively small contribution to the overall errors of $\sim 0.2\,\%$ achieved for CO_2 retrievals. Given that there is scope for further improvement by cooling the detectors this suggests that the SNR on the spectra is high enough that it will not be the limiting factor on the accuracy of retrievals of CO_2 or CH_4 concentrations.

3.5 Resolution and instrument line shape

The maximum resolution of the spectrometer, based on the information on the Fabry–Perot tunable filter provided by the manufacturer, should correspond to a FWHM of 0.10 cm^{-1}. The measured resolution of the instrument, based on the fitting of models to the spectra as described in Sect. 3.3 is a FWHM of about 0.16 cm^{-1}. There are a number of possible reasons why the resolution may fall short of that predicted.

Defects in the FP etalon such as departure from parallelism and reduction in reflectivity may reduce the finesse of the etalon (Tanaka et al., 1995). The manufacturers data is measured with polarized laser light. There are polarization sensitive effects referred to in the Micron optics technical data, that may reduce the performance when using un-polarized light. Resolution could also be reduced as a result of the scan process used in the instrument, due to the etalon spacing changing during integrations as a result of creep effects. Electronic noise or residual ripple on the PZT drive signals could also degrade the resolution.

The theroretical instrument line shape of a FP etalon is described by an Airy function. This has more extended wings than the instrument line shape of a FTS or grating spectrometer. According to Micron Optics the instrument line shapes of their devices agree very well with the theoretical Airy profile. The far wings of the line profile have a significant effect on observed spectra because they can contribute additional light that has the effect of decreasing the apparent strength of observed absorption lines. The total amount of this excess light is determined by the width of the bandpass filter used to isolate the FP order. Any model fitting to spectra must model the full spectral region covered by the filter in order to accurately represent the observed spectrum.

4   Conclusions and future work

A low-cost compact and portable spectrometer for the 1.52–1.67 µm wavelength region has been built and tested. The spectrometer is based on the use of a single-mode fibre Fabry–Perot tunable filter device. The spectrometer has been used in conjunction with a solar tracking system to obtain spectra of the Sun. The spectrometer suffers from drifts in its wavelength calibration due to the phenomenon of creep in the piezoelectric actuator. However, this effect can be corrected by calibrating spectra individually using the known positions of solar spectral lines. The signal to noise ratio of solar spectra is about 700.

It is planned to test the ability of the spectrometer to make accurate measurements of the column abundances of CO_2 and CH_4, by using it alongside a high-resolution Fourier Transform spectrometer. While the current spectrometer appears to have useful capabilities for such work, the analysis of the instrument presented here suggests a number of improvements that could be incorporated in a future version.

The current instrument has a resolution of $0.16\,\mathrm{cm}^{-1}$. However, the tunable filter devices are obtainable with much higher resolutions. Unlike the case with a FTS or grating spectrometer, increasing the resolution would not increase the size of the instrument. A somewhat higher resolution would be desirable to better resolve the actual widths of atmospheric lines. The use of an etalon with similar finesse but higher order to achieve the higher resolution would also reduce the relative size of drifts due to the creep effect.

The temperature dependence of the zero point offset and noise of the detector in the current system, suggests that improved performance would be obtained by moderate cooling of the detector system (e.g. using a thermoelectric cooler) and stabilization of its operating temperature. This would provide both a stable zero point, which is important for accurately measuring line strengths, and lower noise which could enable faster scanning of spectra.

The current instrument requires completely cloud-free skies to produce quality spectra because of its scanning mode of operation. Another improvement would be to feed some of the light into a broad-band detector which measures simultaneously with the narrow-band spectral detector. Corrections could then be made for variations due to thin cloud and aerosols. This would enable operation of the spectrometer in a wider range of conditions.

References

Bailey, J. and Kedziora-Chudczer, L.: Modelling the spectra of planets, brown dwarfs and stars using VSTAR, Mon. Not. R. Astron Soc., 419, 1913–1929, doi:10.1111/j.1365-2966.2011.19845.x, 2012. 1076

Crisp, D.: The Orbiting Carbon Observatory: NASA's first dedicated carbon dioxide mission, in: Sensors, Systems, and Next Generation Satellites XII, edited by: Meynart, R., Neeck, S. P., Shimoda, H., and Habib, S., Proc. SPIE, 710604, doi:10.1117/12.802194, 2008. 1068

Dils, B., De Mazière, M., Müller, J. F., Blumenstock, T., Buchwitz, M., de Beek, R., Demoulin, P., Duchatelet, P., Fast, H., Frankenberg, C., Gloudemans, A., Griffith, D., Jones, N., Kerzen-macher, T., Kramer, I., Mahieu, E., Mellqvist, J., Mittermeier, R. L., Notholt, J., Rinsland, C. P., Schrijver, H., Smale, D., Strandberg, A., Straume, A. G., Stremme, W., Strong, K., Sussmann, R., Taylor, J., van den Broek, M., Velazco, V., Wagner, T., Warneke, T., Wiacek, A., and Wood, S.: Comparisons between SCIAMACHY and ground-based FTIR data for total columns of CO, CH_4, CO_2 and N_2O, Atmos. Chem. Phys., 6, 1953–1976, doi:10.5194/acp-6-1953-2006, 2006. 1068

Gisi, M., Hase, F., Dohe, S., Blumenstock, T., Simon, A., and Keens, A.: XCO_2-measurements with a tabletop FTS using solar absorption spectroscopy, Atmos. Meas. Tech. Discuss., 5, 5691–5724, doi:10.5194/amtd-5-5691-2012, 2012. 1069, 1073

Kawasaki, M., Yoshioka, H., Jones, N. B., Macatangay, R., Griffith, D. W. T., Kawakami, S., Ohyama, H., Tanaka, T., Morino, I., Uchino, O., and Ibuki, T.: Usability of optical spectrum analyser in measuring atmospheric CO_2 and CH_4 column densities: inspection with FTS and aircraft profiles in situ, Atmos. Meas. Tech., 5, 2593–2600, doi:10.5194/amt-5-2593-2012, 2012. 1069

Kenyi, C., Cotton, D. V., and Bailey, J.: Retrieval Software for Total Column Greenhouse Gas Measurements from Ground and Space, Proceedings of the 12th Australian Space Science Conference, submitted, 2013. 1076

Kobayashi, N., Inoue, G., Kawasaki, M., Yoshioka, H., Minomura, M., Murata, I., Nagahama, T., Matsumi, Y., Tanaka, T., Morino, I., and Ibuki, T.: Remotely operable compact instruments for measuring atmospheric CO_2 and CH_4 column densities at surface monitoring sites, Atmos. Meas. Tech., 3, 1103–1112, doi:10.5194/amt-3-1103-2010, 2010. 1069

Livingston, W. L. and Wallace, L.: An Atlas of the Solar Spectrum in the Infrared from 1850 to 9000 cm^{-1} (1.1 to 5.4 microns), N. S. O. Technical Report No 91–001, 1991. 1075, 1076

Petri, C., Warneke, T., Jones, N., Ridder, T., Messerschmidt, J., Weinzierl, T., Geibel, M., and Notholt, J.: Remote sensing of CO_2 and CH_4 using solar absorption spectrometry with a low resolution spectrometer, Atmos. Meas. Tech., 5, 1627–1635, doi:10.5194/amt-5-1627-2012, 2012. 1069

Rothman, L. S., Gordon, I. E., Barbe, A., Benner, D. C., Bernath, P. F., Birk, M., Boudon, V., Brown, L. R., Campargue, A., Champion, J.-P., Chance, K., Coudert, L. H., Dana, V., Devi, V. M., Fally, S., Flaud, J.-M., Gamache, R. R., Goldman, A., Jacquemart, D., Kleiner, I., Lacome, N., Lafferty, W. J., Mandin, J.-Y., Massie, S. T., Mikhailenko, S. N., Miller, C. E., Moazzen-Ahmadi, N., Naumenko, O. V., Nikitin, A. V., Orphal, J., Perevalov, V. I., Perrin, A., Predoi-Cross, A., Rinsland, C. P., Rotger, M., Šimečková, M., Smith, M. A. H., Sung, K., Tashkun, S. A., Tennyson, J., Toth, R. A., Vandaele, A. C., and Vander Auwera, J.: The HI-TRAN 2008 molecular spectroscopic database, J. Quant. Spectrosc. Ra., 110, 533–572, doi:10.1016/j.jqsrt.2009.02.013, 2009. 1076

Suto, H., Kuze, A., Shiomi, K., and Nakajima, M.: On orbit status of TANSO-FTS on GOSAT, in: Sensors, Systems, and Next Generation Satellites XIV, edited by: Meynart, R., Neeck, S. P., Shimoda, H., Proc. SPIE, 782604, doi:10.1117/12.865214, 2010. 1068

Tanaka, M., Yamashita, T., Sato, S., and Okuda, H.: A Fabry–Perot spectrometer for near-infrared astronomical observations, Publ. Astron. Soc. Pac., 97, 1020–1025, 1985. 1079

Washenfelder, R. A., Toon, G. C., Blavier, J.-F., Yang, Z., Allen, N. T., Wennburg, P. O., Vay, S. A., Matross, D. M., and Daube, B. C.: Carbon dioxide column abundances at the Wisconsin Tall Tower site, J. Geophys. Res., 111, D22305, doi:10.1029/2006JD007154, 2006. 1078

Wilson, E. L., Georgieva, E. M., and Heaps, W. S.: Development of a Fabry–Perot interferometer for ultra-precise measurements of column CO_2, Meas. Sci. Technol., 18, 1495–1502, doi:10.1088/0957-0233/18/5/040, 2007. 1069

Wunch, D., Toon, G. C., Blavier, J.-F. L., Washenfelder, R. A., Notholt, J., Connor, B. J., Griffith, D. W. T., Sherlock, V., and Wennberg, P. O.: The total carbon column observing network, Philos. T. Roy. Soc. A., 369, 2087–2112, doi:10.1098/rsta.2010.0240, 2010. 1068, 1078

Table 1. Fabry–Perot tunable filter parameters.

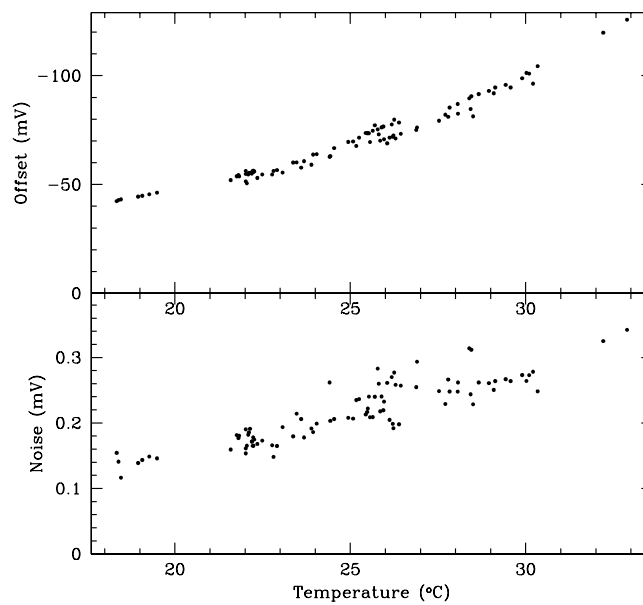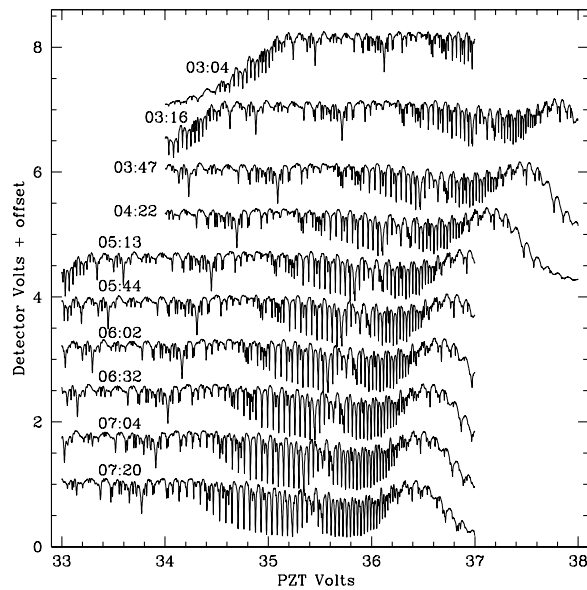|	
Wavelength range	1.52–1.64 µm
Bandwidth	3.03 GHz
Free spectral range	0.124 µm
Finesse	5348
Insertion loss	2.8–3.3 dB
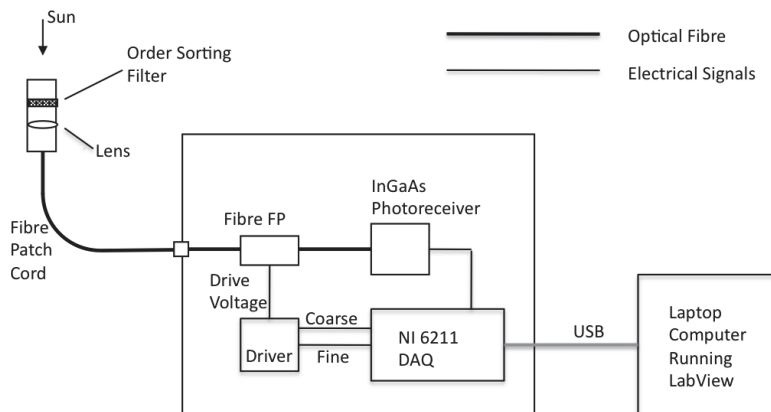
Fig. 1. Main components of spectrometer system.
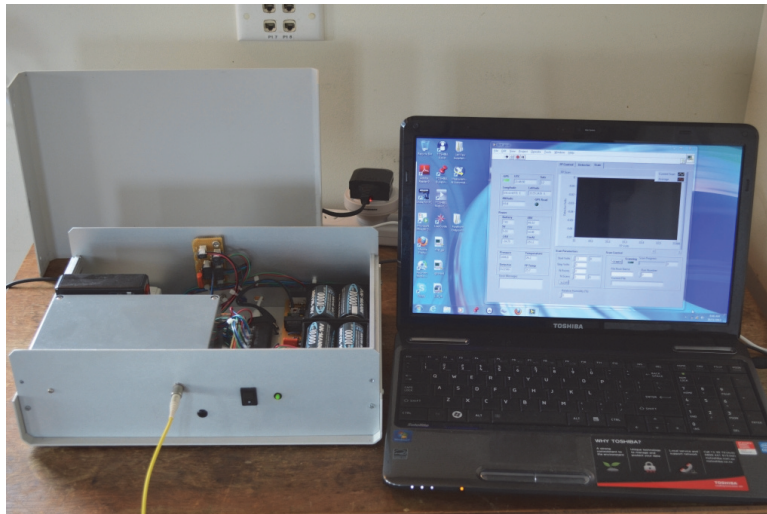
Fig. 2. The spectrometer and its control computer.

**Fig. 3.** Zero point offset of the detector and detector noise as a function of temperature.

Fig. 4. Raw data from the spectrometer after zero point correction showing a series of spectra recorded on 4 October 2012. The spectra are labelled by the UTC of the start of scan. All but the last spectrum are offset vertically to avoid overlap.
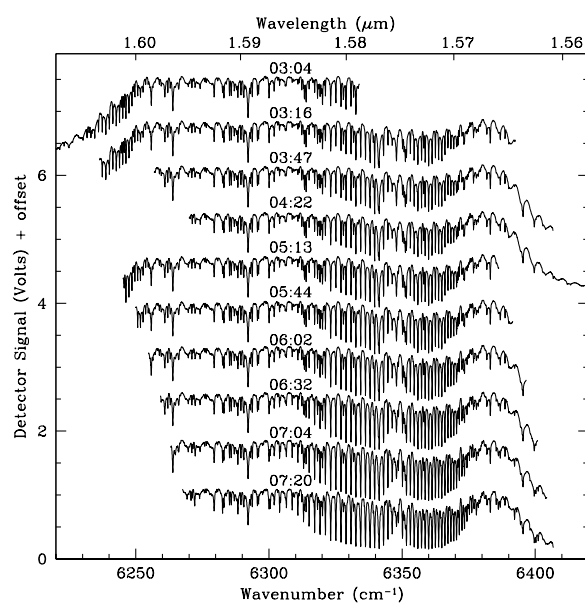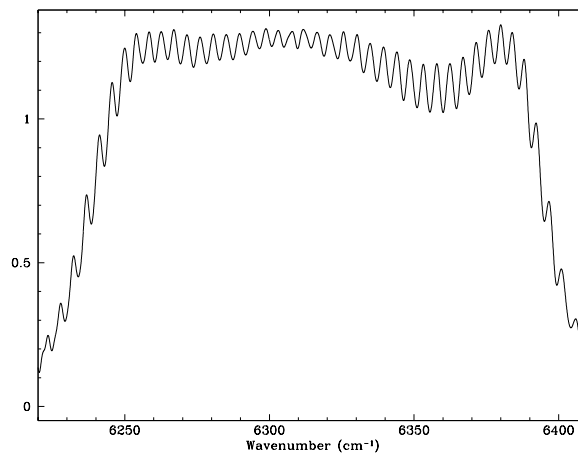
Fig. 5. The same set of spectra as in Fig. 4 after calibration in wavenumber. All but the last spectrum are offset vertically to avoid overlap.
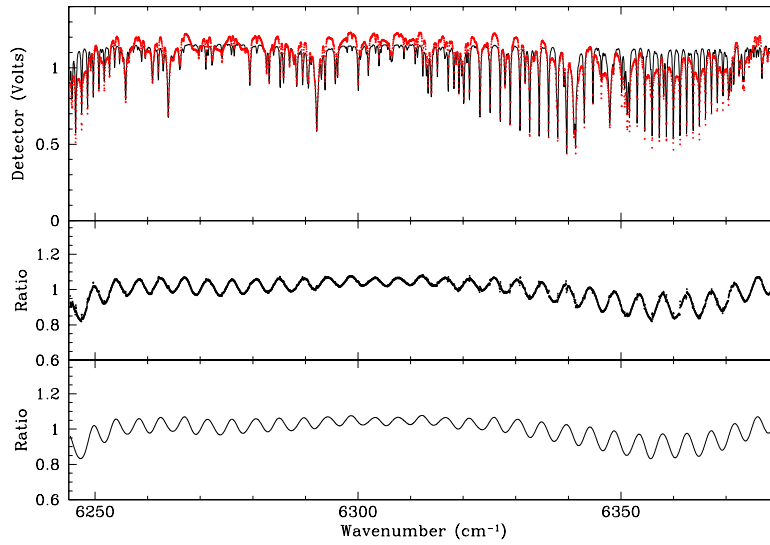
Fig. 6. Illustration of procedure used to determne the filter calibration. The red points are an observed spectrum and the black line is a model spectrum derived as described in the text. The middle panel shows the result of dividing the observed spectrum by the model. The lower panel is the result of Fourier filtering this to leave only low frequency structure which is the required calibration curve.

Fig. 7. Instrument response function for the 1.58 μm order sorting filter.

Fig. 8. Final result of correcting the spectra from Fig. 5 using the instrument response function. All but the last spectrum are offset vertically to avoid overlap.

Fig. 9. Comparison of a small section of three different observed spectra in the same wavelength region illustrating SNR in the spectra. Three different spectra are shown in black, green and red. The lower panel shows the differences (red–black) and (green–black). The spectral features that show up in the difference spectra are telluric absorption lines that increase in strength due to the changing zenith angle.